Dark cytotoxicity beyond photo-induced one of silica nanoparticles incorporated with RuII nitrosyl complexes and luminescent Mo6I8 cluster units

Olga Bochkova, Svetlana Fedorenko, Artem Mikhailov, Gennadiy Kostin, Maxim Mikhailov, Maxim Sokolov, Julia Elistratova, Kirill Kholin, Maxim Tarasov, Yulia Budnikova, et al.

Journal of Photochemistry & Photobiology, A: Chemistry 446 (2024) 115147

Contents lists available at ScienceDirect

Journal of Photochemistry & Photobiology, A: Chemistry

journal homepage: www.elsevier.com/locate/jphotochem

Dark cytotoxicity beyond photo-induced one of silica nanoparticles incorporated with Ru^{II} nitrosyl complexes and luminescent $\{Mo_6I_8\}$ cluster units

Olga Bochkova [a,*], Svetlana Fedorenko [a], Artem Mikhailov [b,c], Gennadiy Kostin [c], Maxim Mikhailov [c], Maxim Sokolov [c], Julia Elistratova [a], Kirill Kholin [d], Maxim Tarasov [a], Yulia Budnikova [a], Guzel Sibgatullina [e], Dmitry Samigullin [e], Irek Nizameev [a], Vadim Salnikov [e], Ivan Yakovlev [c], Darina Rozhentsova [f], Anna Lyubina [a], Syumbelya Amerhanova [a], Alexandra Voloshina [a], Tatiana Gerasimova [a], Asiya Mustafina [a]

[a] Arbuzov Institute of Organic and Physical Chemistry, FRC Kazan Scientific Center of RAS, Arbuzov str., 8, 420088 Kazan, Russia
[b] Université de Lorraine, CNRS, CRM2, UMR 7036, Nancy 54000, France
[c] Nikolaev Institute of Inorganic Chemistry SB RAS, 3, Acad. Lavrentiev Ave., Novosibirsk 630090, Russia
[d] Kazan National Research Technological University, Department of Physics, Karl Marx str., 68, 420015 Kazan, Russia
[e] Kazan Institute of Biochemistry and Biophysics, FRC Kazan Scientific Center of RAS, 2/31 Lobachevski str., 420111 Kazan, Russia
[f] Kazan (Volga Region) Federal University, 18 Kremlyovskaya str., 420008 Kazan, Russia

ARTICLE INFO

Keywords:
Nitrosyl ruthenium
Silica nanoparticles
Photochemistry
Cytotoxicity
Hexamolybdenum cluster
Cell visualization

ABSTRACT

The present work reports the synthesis of the silica nanoparticles (SNs) incorporated by two photoactive components, which are the representatives of Ru^{II} nitrosyl complexes and $[\{Mo_6I_8\}(CH_3COO)_6]^{2-}$ cluster units. The Ru^{II} nitrosyl complexes are incorporated through the doping procedure into the SNs. The embedding of amino-groups onto the Ru^{II}-doped SNs facilitates the deposition of the cluster units, thus, resulting in the heterometallic core–shell SNs. Combination of the two photoactive components in the SNs results in the anti-synergistic effect on the photochemical and photodynamic activities of the Ru^{II} and $\{Mo_6I_8\}$-based complexes correspondingly. The enhanced leaching of the cluster units from the heterometallic SNs correlates with the nitrosyl → nitro transformation of the encapsulated Ru^{II} nitrosyl complexes. The formation of the so-called protein corona onto the heterometallic SNs is revealed as the reason for high colloid stability and efficient cell internalization, which is visualized through the red emission of the $\{Mo_6I_8\}$-clusters. The cytotoxicity measurements reveal both synergistic effect of both components on the cytotoxicity evaluated in the so-called dark conditions and anti-synergistic effect on the photo-induced cytotoxicity. The significant dark cytotoxicity of the heterometallic SNs correlates with their high internalization and the enhanced leaching of the cluster units.

1. Introduction

Silica-based nanoarchitectures play an important role in design and development of functional nanomaterial for therapeutic activity, which is well exemplified by the recently published reports [1–8]. Silica nanoparticles (SNs) itself can affect a cell viability due to great activity of the interfacial silanol groups, although the surface modification by amino-groups can significantly smooth out this effect [9,10]. Great diversity of functional properties of metal complexes incorporated into silica nanoparticles allows to gain in their therapeutic activities [11,12], while the permeability of silica matrix to small molecules and ions provides a prerequisite for a development of the so-called hollow nanoarchitectures [13] and drug delivery systems [1–4].

The photo-induced NO release by ruthenium nitrosyl complexes is represented by great number of reports demonstrating structure impact on the photo-induced NO release [14–24]. The electrochemical reduction of Ru^{II} nitrosyl complexes *via* electron deficient NO^+ ligand is one more trigger of the release of NO [20]. It is also worth noting the acidification as another factor facilitating the release of NO as it is demonstrated for $[RuNO(NH_3)_5]^{3+}$ complex [25]. Thus, the photo-

* Corresponding author.
E-mail address: o.d.bochkova@mail.ru (O. Bochkova).

https://doi.org/10.1016/j.jphotochem.2023.115147
Received 2 May 2023; Received in revised form 21 August 2023; Accepted 31 August 2023
Available online 3 September 2023

irradiation, electrochemical reduction and acidification are the possible triggers of the NO release. The release of NO induced by the external stimuli can be a reason for the cytotoxicity of Ru^{II} nitrosyl complexes [14,21,26–28]. Moreover, the interaction of Ru(II) nitrosyl complexes with DNA molecules can also provide a basis for the cytotoxicity of the complexes [29].

It is worth noting the reports demonstrating both encapsulation of ruthenium nitrosyl complexes into phospholipid vesicles [27,28], F-127-based micelles [23,30] and immobilization of the complexes at the modified surface of mesoporous silica nanoparticles [31] as the tools for development of nanomaterial with photo controlled NO release. The already documented procedures of the incorporation of Ru^{II} nitrosyl complexes into silica nanoparticles are represented by the synthetic routes avoiding the use of ammonia for a catalysis of hydrolysis of TEOS, although high polydispersity indices and great size-values are the shortcoming of such nanoarchitectures [32,33]. For the best of our knowledge, an inclusion of photochemically active Ru^{II} nitrosyl complexes into SNs *via* the synthetic routes based on the ammonia-catalyzed hydrolysis of TEOS is rather poor documented in literature. Moreover, the specific surface modification of silica nanoparticles loaded with Ru^{II} nitrosyl complexes can enhance their intracellular penetration [34,35]. It is also worth noting the synthetic route of the deposition of luminescent cluster complexes onto the surface of amino-decorated SNs [12], which allows to combine them with Ru^{II} nitrosyl complexes included into the composite SNs.

The choice of $[Ru(NO)(NH_3)_2Py_2(NO_3)](NO_3)_2$ (**1**), $[Ru(NO)(NH_3)_4OH]Cl_2$ (**2**) and $[Ru(NO)Py_4OH](PF_6)_2$ (**3**) is affected by the previous reports revealing the efficacy of related complexes in the NO-generation [36,37]. The complexes are included into amino-modified SNs (monometallic SNs) followed by the incorporation of luminescent $[\{Mo_6I_8\}(CH_3COO)_6]^{2-}$ clusters onto the surface of amino-modified SNs, thus, resulting in the heterometallic SNs. The ability of the complexes to photo- and redox-induced release of NO in the aqueous solutions is compared with that of the complexes incorporated into the monometallic and heterometallic SNs. The combination of the efficient red luminescence fitting to the so-called biological window of transparency of $[\{Mo_6I_8\}(CH_3COO)_6]^{2-}$ clusters makes them convenient choice for combination with Ru(II) nitrosyl complexes in the heterometallic SNs.

The cytotoxicity of the monometallic and heterometallic SNs is demonstrated for the cancer and normal cell lines in both dark and irradiated conditions. The insignificant cytotoxicity of the SNs loaded with Ru^{II} nitrosyl complexes is enhanced after the amino-modification of their surface. The red luminescence of the cluster units deposited onto the amino-modified surface allows to reveal their cellular internalization. The cytotoxicities of the composite SNs measured both under and without irradiation are correlated with their leaching capacity in the solutions modeling the biological liquids.

2. Materials and method

2.1. Materials

Commercial chemicals tetraethyl orthosilicate (TEOS) 98%, ammonium hydroxide (28–30%), *n*-heptanol 98%, cyclohexane 99%, hexane (97%), acetone (99%), 3-aminopropyltriethoxysilane (APTES, 99%), β-alanine and fluorescamine were purchased from Acros Organics. Triton X-100 (98%), Bovine serum albumin (≥98 %), Dulbecco Phosphate Buffered Saline (DPBS), 5,5- dimethyl-pyrroline N-oxide (DMPO), 4′,6-Diamidino-2-phenylindole dihydrochloride (DAPI), propidium iodide, Griess reagent and L-Glutathione reduced (GSH, 98%)were purchased from Sigma-Aldrich. $Mn(NO_3)_2{\cdot}4H_2O$ was purchased from Alfa Aesar. Ethanol and TEOS were purified by distillation.

Ruthenium complexes $[Ru(NO)(NH_3)_2Py_2(NO_3)](NO_3)_2$ (**1**) [38], $[Ru(NO)(NH_3)_4OH]Cl_2$ (**2**) [39] and $[Ru(NO)Py_4OH](PF_6)_2$ (**3**) [40] were synthesized according to the reported procedures. The cluster complex $(n\text{-}Bu_4N)_2[\{Mo_6I_8\}(CH_3COO)_6]$ (**{Mo_6I_8}**) was synthesized in accordance with the previously published procedures [41]. IR-spectra and XRD powder patterns confirmed purity of the samples.

Phosphate (pH 6.85) and acetic/acetate (pH 4.50) buffers were used to adjust the required pH-values.

Griess reagent was prepared by dissolution of 0.5 g of the reagent, consisting of 1-naphthylamine, sulfanilamide and tartaric acid (1%:10%:89%) mixture, in 5 mL of bidistilled water. For the calibration purposes, the absorbance at 522 nm versus $NaNO_2$ concentration was determined in the presence of Griess reagent (0.12 mL). The solution of test sample ($5{\bullet}10^{-5}$ M of aqueous solution of Ru nitrosyl complexes **1**, **2** or **3**; 0.4 $g{\bullet}L^{-1}$ of silica nanoparticles) and Griess reagent (0.12 mL) was irradiated by LED 405 nm, 50 mW in a cuvette in order to determine the nitric oxide yield.

2.2. Synthesis

The synthesis of **1**(**2** or **3**)@SNs through the water-in-oil microemulsion method the synthetic mixture of Triton X-100 (4.76 g), *n*-heptanol (4.58 mL), cyclohexane (18.64 mL), NH_3 (28–30%, 0.4 mL) and aqueous solution of Ru nitrosyl complexes **1**, **2** or **3** (0.01 M, 2.2 mL). The obtained microemulsion was then mixed for 30 min. Afterwards, the solution formed by mixing of Triton X-100 (4.76 g), n-heptanol (4.58 mL), cyclohexane (18.64 mL) and TEOS (0.4 mL) was added dropwise to the previously prepared microemulsion. After 24 h of stirring silica nanoparticles were precipitated from microemulsion with acetone, centrifuged and washed 1 time with ethanol/acetone mixture (1:1), 1 time with ethanol and 3 times with doubly distilled water. After each washing step the solution of silica nanoparticles was ultrasonicated without heating for 10 min.

For synthesis of **1**(**2** or **3**)@SN-NH_2 the water-in-oil microemulsion was prepared by mixed of 67.5 mL of cyclohexane, 17.25 g of Triton X-100, 16.2 mL of heptanol, 4.32 mL of Ru^{II} nitrosyl complexes **1**, **2** or **3** (C = 0.01 M) in a reaction flask. After 15 min of mixing, 0.54 mL of NH_3 (28–30%) was added, and after another 15 min 0.45 mL of TEOS was added. The obtained solution was left to stir for 24 h, after which 0.45 mL of TEOS and 0.09 mL of APTES were added and stirred for 24 h. The synthesized silica nanoparticles were precipitated with acetone and separated by centrifugation. Purification of the as-prepared SNs was carried out according to the standard procedure. The obtained nanoparticles were washed 1 time with a mixture of ethanol-acetone (1:1), 1 time with ethanol, 3 times with doubly distilled water. After each washing step the solution of silica nanoparticles was ultrasonicated without heating for 10 min.

The synthesis of **1**(**2** or **3**)@SN-NH_2-$\{Mo_6I_8\}$ was carried out by adsorption of cluster anions $[\{Mo_6I_8\}(CH_3COO)_6]^{2-}$ on **1**(**2** or **3**)@SN-NH_2 nanoparticles according to the following procedure: the aqueous solution of the cluster complexes (0.035 mM) was mixed with the aqueous colloids of the **1**(**2** or **3**)@SN-NH_2 (0.5 $g{\cdot}L^{-1}$). The mixture was stirred by means of Shaker Hei-MIX Multi Reax for 10 min and sonicated for 15 min with further phase separation by centrifugation at 4° C (15000 rpm). Afterwards, the assembled nanoparticles were washed by water and dispersed in water.

The fluorescence procedure with the use of fluorescamine was used for quantitative analysis of amino groups on the surface of silica nanoparticles (Table S1, Fig. S1) [42].

To determine the release of both Ru^{II} nitrosyl and $\{Mo_6I_8\}$ cluster complexes from the SNs aqueous dispersions of SNs (0.5 gL^{-1}) was continuously stirred in phosphate buffer (pH 6.8, 0.01 M), in acetate buffer (pH 4.5, 0.01 M), or in glutathione (GSH, 0.01 M in phosphate buffer pH 6.8) solution during 24 h. Then, the aqueous dispersions of the SNs were centrifuged (15 min, 15000 rpm, 4 °C). The transparent supernatant solutions and silica nanoparticles were analyzed separately.

2.3. Methods

The detailed description of the common methods (ICP-OES, TEM, UV–Vis, IR, luminescence, ESR spectroscopy, pH- potentiometric and electrochemical methods), is represented in ESI data.

Cytotoxic effects of samples on human cancer and normal cells were estimated by means of the multifunctional Cytell Cell Imaging system (GE Health Care Life Science, Sweden) using the Cell Viability Bio App which precisely counts the number of cells and evaluates their viability from fluorescence intensity data [43]. The M-HeLa clone 11 human, epithelioid cervical carcinoma, strain of HeLa, clone of M-HeLa; WI-38 VA-13 cell culture, subline 2RA (human embryonic lung) from the Type Culture Collection of the Institute of Cytology (Russian Academy of Sciences) and Chang liver cell line (Human liver cells) from N. F. Gamaleya Research Center of Epidemiology and Microbiology were used in the experiments. The cells were cultured in a standard Eagle's nutrient medium manufactured at the Chumakov Institute of Poliomyelitis and Virus Encephalitis (PanEco company) and supplemented with 10% fetal calf serum and 1% nonessential amino acids. The cells were plated into a 96-well plate (Eppendorf) at a concentration of 1×10^5 cells mL^{-1}, 150 μL of medium per well, and cultured in a CO_2 incubator at 37 °C. Twenty four hours after seeding the cells into wells, the compound under study was added at a preset dilution, 150 μL to each well. The dilutions of the compounds were prepared immediately in nutrient media. The experiments were repeated three times. Intact cells cultured in parallel with experimental cells were used as a control.

Photo-induced cytotoxicity of **1**(**2** or **3**)@SN-NH_2 and **1**(**2** or **3**)@SN-NH_2-{Mo_6I_8} nanoparticles in relation to M-HeLa cancer cell and Chang Liver cell lines was studied under irradiation light emitting diode (405 nm, 50 mW) for 30 min.

The uptake of **1**(**2** or **3**)@SN-NH_2-{Mo_6I_8} by M-HeLa and Chang Liver cells was analyzed using flow cytometry (Guava easy Cyte 8HT, USA). Flow cytometry was used to generate statistics on the uptake of the test nanoparticles by cancer and living cells. Untreated cells were used as negative control. M-HeLa cells at $1x10^5$ cells / well and Chang Liver cells at $1x10^5$ cells / well were plated into 6-well plates to a final volume of 2 mL. After a 24-hour incubation, solution of **1**(**2** or **3**)@SN-NH_2-{Mo_6I_8} (0.25 gL^{-1}) was added to the M-HeLa cells and Chang Liver cells and incubated for 24 h in a CO_2 incubator.

Fluorescence microscopy images were obtained by using both Nikon Eclipse Ci-S fluorescence microscope (Nikon, Japan,) at 400x magnification and Leica TCS SP5 confocal microscope (Leica Biosystems, Germany) at 1000x magnification and then analyzed using Las AF and Las X software packages (Leica Biosystems, Germany). Multiphoton laser was used for detection of fluorescence: for DAPI excitation was 400 nm and the emission was in a range 430–550 nm, signal from compounds was excited at 380 nm and the fluorescence emission was collected from 600 to 670 nm. M-HeLa cells at 1×10^5 cells / well in a final volume of 2 mL were seeded into 6-well coverslip plates at the bottom of each well. After 24 h of incubation, solutions of the studied **1**(**2** or **3**)@SN-NH_2-{Mo_6I_8} (0.25 and 0.12 gL^{-1}) were added to the wells and cultured for 24 h in a CO_2 incubator. Then, M-HeLa cells were fixed and stained with DAPI (blue, cell nucleus staining).

The EDX analysis **1**@SN-NH_2 and **1**@SN-NH_2-{Mo_6I_8} nanoparticles was examined by electron microscopy using a Hitachi HT7800 transmission electron microscope (Hitachi High-Tech Science Corporation, Japan). 5 μL of the aqueous dispersions of **1**@SN-NH_2 and **1**@SN-NH_2-{Mo_6I_8} (0.5 gL^{-1}) was applied straight to on a 3.05 mm in diameter copper grid with a formvar film (01700-F, Ted Pella, Inc.) and dried at room temperature. The grid with the dried sample was placed in the transmission electron microscope using a special holder, followed by imaging at an accelerating voltage of 80 kV in the TEM mode. Elemental analysis of particles was carried out using the Microanalysis system AZtecEnergy TEM Advanced with detector Ultim Max TEM / AZtecEnergy TEM Advanced with Ultim Max TEM (Microanalysis system mounted on Hitachi HT7800 electron microscope).

3. 3.Results and discussion

3.1. Synthesis of RuNO-based nanocomposites and their irradiation-induced transformations

The synthesis of the SNs loaded with the complexes **1**, **2** and **3** was performed *via* the modified microemulsion procedure (for the details see Experimental Section). The synthesis of the monometallic SNs, which herein and further will be designated as **1**(**2** or **3**)@SNs is schematically illustrated by Fig. 1a. The growth of silica nanostructures in the framework of the microemulsion procedure requires an aqueous ammonia, which can trigger a modification of the ruthenium complexes. The monitoring of the electronic absorption spectra of complexes **1**, **2**, **3** in aqueous and aqueous ammonia solutions (Fig. 1b-d) argues for their inner-sphere transformations in the aqueous ammonia, which can derive from a ligand exchange [30,44] or/and pH dependent NO-NO_2 equilibrium (1) [45–47].

$$\{Ru^{2+}\text{-}NO^{+}\} + HO^{-} = \{Ru^{2+}\text{-}NO_2^{-}\} + H^{+} \quad (1)$$

However, the storage of the complexes in the aqueous ammonia solutions for one day doesn't induce further significant spectral changes even when the solutions are not shielded from the sunlight.

The successful loading of the complexes into SNs is evident from the Si:Ru molar ratios calculated from the data of ICP-OES method (Table 1). The ICP-OES analysis of the composite SNs revealed the Si:Ru molar ratios on the level comparable with those previously reported for the composite SNs loaded with $[Ru(dipy)_3]^{2+}$ complexes [48]. Moreover, the transparency of silica matrix allows to monitor the spectral features of the complexes within SNs (Fig. 2 a-c, Fig. S2), which reveal the similarity with the spectra of the complexes in the aqueous ammonia solutions illustrated in Fig. 1b-d.

The average diameter values of the composite SNs (d^{TEM}) evaluated by transmission electronic microscopy (TEM) data are collected in Table 1. The data (Table 1) indicate that the size values of **1**(**2** or **3**)@SNs are smaller than those of **1**(**2** or **3**)@SNs-NH_2 due to some difference in the synthetic protocols (for more details see the Experimental Section). Fig. 2 (panels d, e) exemplifies the TEM images for **2**@SNs and **2**@ SNs-NH_2, the TEM images of **1**(**3**)@SNs and **1**(**3**)@SNs-NH_2 are presented in Fig.S3.

The characterization of **1**(**2** or **3**)@SNs by DLS method indicates the significant aggregation of **1**(**3**)@SNs derived from the surface neutralization of the SNs, since the electrokinetic potential values of **1**(**3**)@SNs are close to zero (Table 1), while the colloid behavior of **2**@SNs is similar with that of the pristine SNs due to the negative ζ-value (about −30 mV) [49]. Commonly, amino-modified SNs demonstrate high aggregation arisen from ζ-values close to zero, since the surface exposed protonated ammonium groups provide the surface neutralization, and the positive recharging of the amino-modified surface requires the acidification [12,50]. However, the amino-modified analogues **1**(**2** or **3**)@SNs-NH_2 exhibit rather low aggregation due to the high positive surface charging as it is evident from the corresponding ζ-values (Table 1). It is worth assuming that the enhanced positive charge of **1**(**2** or **3**)@SNs-NH_2 derives from the protonation of the surface exposed amino-groups due to the nitrosyl-nitro transformation (1) of the complexes.

The IR spectroscopy analysis reveals the band at 1934, 1844 and 1866 cm^{-1} peculiar for the nitrosyl ligands ν(NO) in complexes **1**, **2** and **3** correspondingly, whereas the band shifts to ~1890 cm^{-1} in the composite SNs (Fig. 3a). The difference in the ν(NO) values in complexes **1, 2, 3** derives from the different nature of the ancillary ligands, whereas, the observed changes in the ν(NO) values of the complexes after their incorporation into the SNs indicate the inner-sphere rearrangements, which are beyond the framework of nitrosyl-nito transformations. This confirms the above mentioned assumption on the ligand exchange as one more reason besides nitrosyl-nitro transformations for the inner-sphere rearrangements evident from the

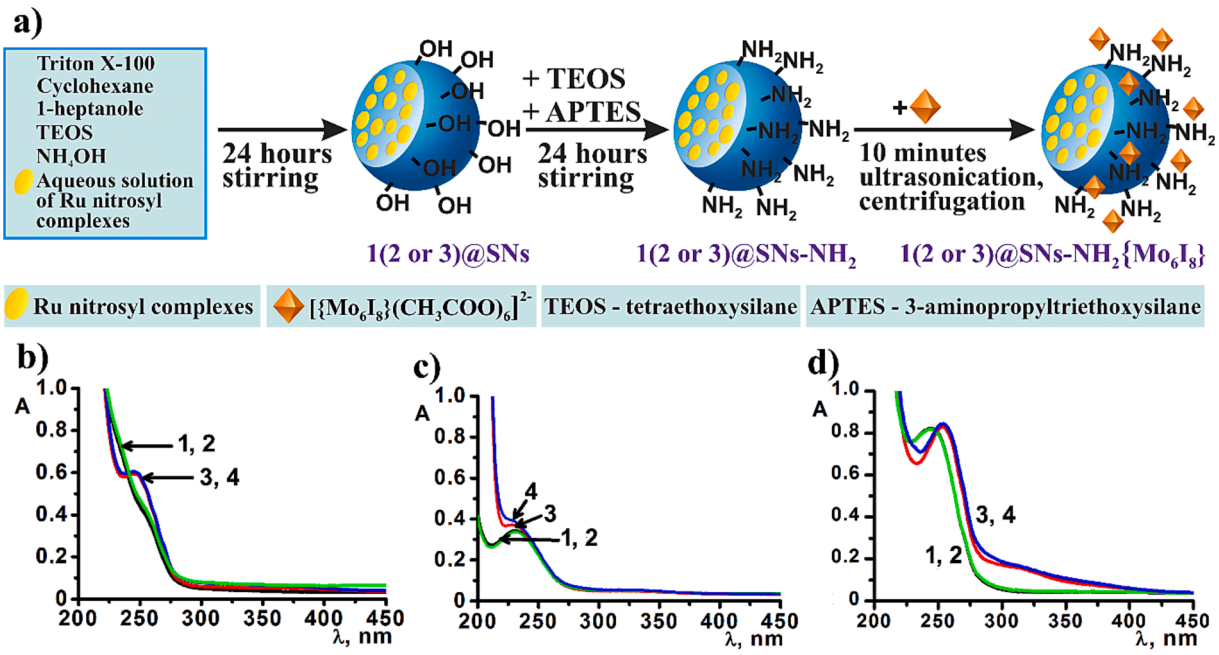

Fig. 1. (a) The schematic illustration of the synthesis of the composite SNs. UV–vis spectra of aqueous solutions of complexes **1** (C = 0.05 mM) (b), **2** (C = 0.058 mM) (c) and **3** (C = 0.044 mM) (d): fresh prepared – 1 (black); after 24 h – 2 (green) and in the presence of NH_4OH fresh prepared – 3 (red) and after 24 h – 4 (blue).

Table 1
Values of averaged diameter (d^{TEM}) evaluated by TEM method and averaged hydrodynamic diameter by Volume (d^{DLS}), polydispersity index (**PDI**) and ζ-potential values evaluated by DLS technique for different systems and also Si:Ru:Mo molar ratio obtained by ICP-OES technique.

Sample	d^{TEM}, nm	d^{DLS}, nm	PDI	ζ, mV	Si:Ru:Mo
1@SNs	33 ± 2	1570 ± 178	0.310	−13	1:0.012
2@SNs	42 ± 5	86 ± 1	0.111	−30	1: 0.014
3@SNs	35 ± 3	187 ± 14	0.170	6	1: 0.014
1@SNs-NH_2	40 ± 3	117 ± 2	0.151	25	1:0.014
2@SNs-NH_2	56 ± 6	99 ± 2	0.175	27	1:0.015
3@SNs-NH_2	40 ± 3	171 ± 1	0.199	27	1:0.012
1@SNs-NH_2-{Mo_6I_8}	42 ± 4	950 ± 50	0.9	13	1:0.013:0.013
2@SNs-NH_2-{Mo_6I_8}	56 ± 6	655 ± 10 and 917 ± 60	0.9	7	1:0.014:0.011
3@SNs-NH_2-{Mo_6I_8}	40 ± 3	868 ± 40	0.7	7	1:0.012:0.011
1@SNs-NH_2-{Mo_6I_8} + BSA	–	299 ± 15	0.263	−20	–
2@SNs-NH_2-{Mo_6I_8} + BSA	–	350 ± 20	0.188	–23	–
3@SNs-NH_2-{Mo_6I_8} + BSA	–	342 ± 18	0.228	−20	–

spectral changes of the complexes after their incorporation into the SNs (Fig. 2). It is worth noting that ancillary ligand exchange and nitrosyl-nitro transformations occur simultaneously, and their mutual influence is difficult to assess. Unfortunately, all other IR bands corresponding to complexes are overlapped by bands of SiO_2.

The photochemical transformations followed by the release of NO from the complexes in aqueous solutions were manifested by the significant changes in their spectral behavior [45,51,52], which are represented in Fig. 3. The light-induced release of NO is confirmed by the spectrophotometry technique with the use of Griess reagent (GR) [53]. The photo-induced spectral changes of the complexes and the release of NO measured by the GR-analysis are represented in Fig. 3b-d and Fig. 4a.

The complexes within **1**(**2** or **3**)@SNs demonstrate poor photo-induced spectral changes (Fig. S2) with no detectable release of NO due to the Griess analysis (Fig. 4a). Moreover, the IR-analysis of **1**(**2** or **3**)@SNs separated from the aqueous dispersions after their light irradiation for one hour reveals the bands of the nitrosyl ligands (Fig. S4). This indicates that the release of NO is slowed down for the complexes located in the interior of the SNs. It is worth noting that loading of SNs with molecular complexes derives from their dehydration and aggregation in a silica confinement [54,55]. In turn, the insufficient hydration of the complexes inside silica matrix can be a factor facilitating the reestablishment of the initial Ru^{II} nitrosyl complex in accordance with the equilibrium (2).

$$[Ru^{II}NO^{+}(L)_4(X)]^{2+} + h\nu + H_2O = [Ru^{III}(L)_4(X)(H_2O)]^{2+} + NO^0 \quad (2)$$

It is worth noting that the uploading of SNs by molecular complexes commonly results in their distribution within both core and shell zones of silica spheres [56]. In turn, the exterior located complexes should be greatly hydrated than those located in the interior of the SNs. However, the exterior complexes contribute very poor if any to the photo-induced spectral changes. This allows to assume that the exterior complexes due to the greater exposure to the ammonia-based synthetic solution exhibit more pronounced nitrosyl-nitro transformation than those localized in the interior of the SNs. The photo-induced spectral changes of **1**(**2** or **3**)@SNs-NH_2 (Fig. 2a-c) are less pronounced than in the case of **1**(**2** or **3**)@SNs, which agrees well with their longer (48 h for **1**(**2** or **3**)@SNs-NH_2 instead of 24 h for **1**(**2** or **3**)@SNs) exposure to the alkaline synthetic media. The spectral data are confirmed by the Greiss analysis results (Fig. 4a).

*3.2. Redox-induced transformations of complexes **1–3** and **1**(**2** or **3**)@SNs-NH_2*

The redox-induced transformations of complexes **1**–**3** are characterized by the number of successive reduction stages (Fig. S5). During the reduction process, an intense gas evolution is observed at the electrode already at the first peak potential, which can be explained by the evolution of gaseous nitric oxide (NO). This agrees well with the literature data postulating for similar $[Ru^{II}\text{-}NO]^{3+}$ complexes the one-electron reductive process centered at the nitrosyl ligand [57,58] as the reason for NO release. The similar electrochemical behavior is

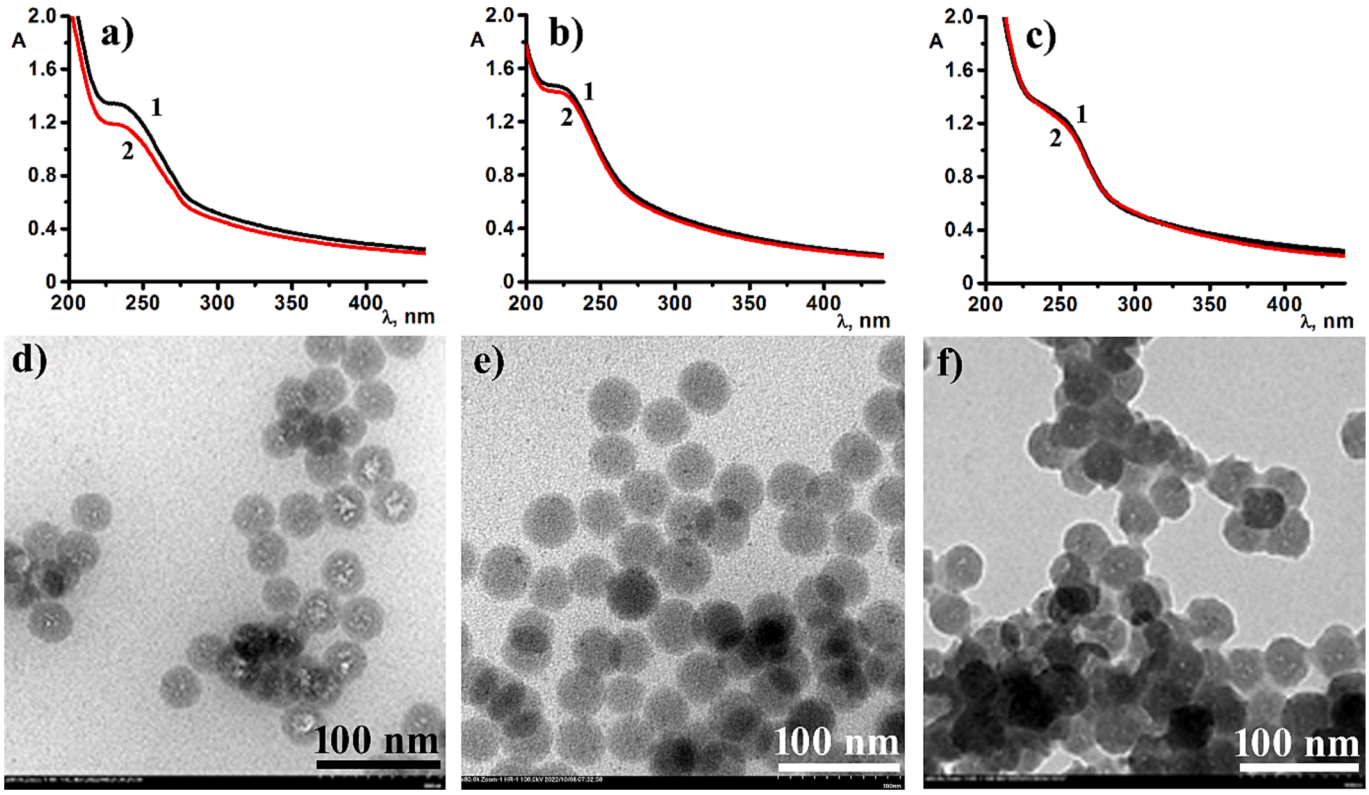

Fig. 2. UV–visible spectra of aqueous dispersions of (**1**–**3**)@SNs-NH_2 (a-c) before (1) and after 1 h of irradiation (2) (405 nm). TEM-images of **2**@SNs (d), **2**@ SNs-NH_2 (e), **2**@SNs-NH_2-{Mo_6I_8} (f).

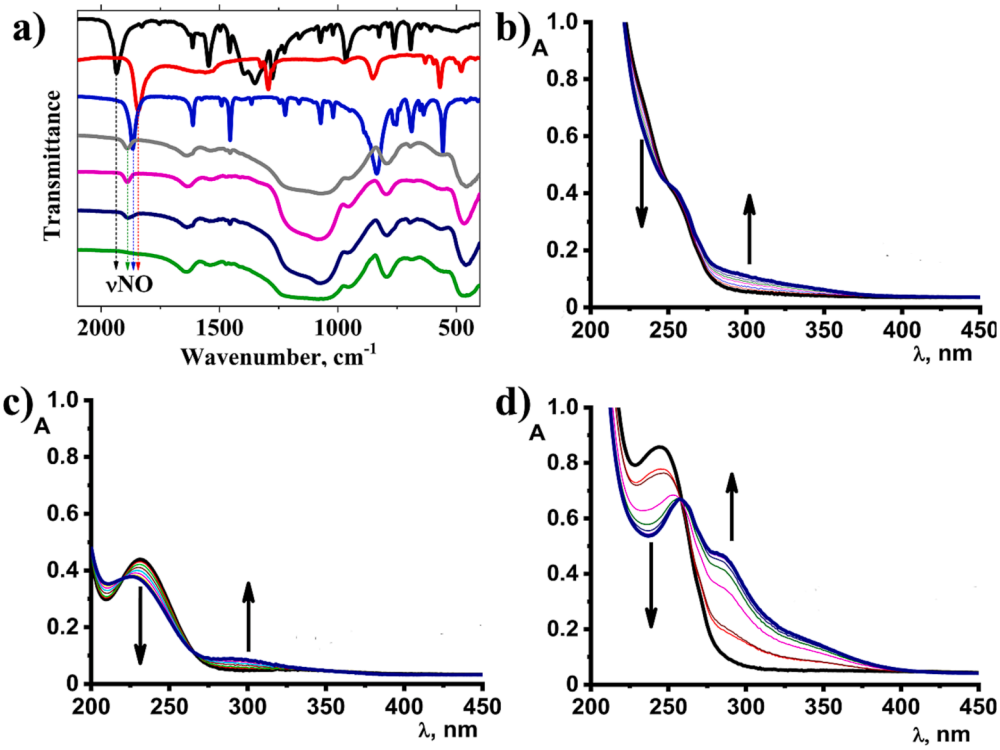

Fig. 3. (a) Infrared spectra of complexes **1** (black), **2** (red), **3** (blue) and silica nanoparticles **1**@SNs-NH_2 (grey), **2**@SNs-NH_2 (magenta), **3**@SNs-NH_2 (navy) and pristine SNs-NH_2 (green). (b-d) UV–Vis spectra of complexes **1** (b), **2** (c) and **3** (d) in aqueous solutions recorded during 60 min of irradiation (405 nm).

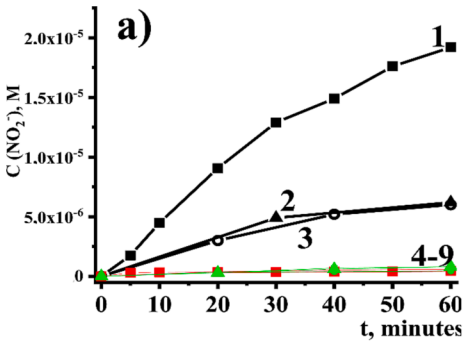

b)

Sample	$-E_p^1$	$-E_p^2$	$-E_p^3$
1	0.53	1.78	-
1@SNs-NH_2	1.29	2.36	-
2	1.22	1.87	2.32
2@SNs-NH_2	1.04	1.88	2.98
3	0.66	1.77	3.01
3@SNs-NH_2	0.93	2.10	2.87

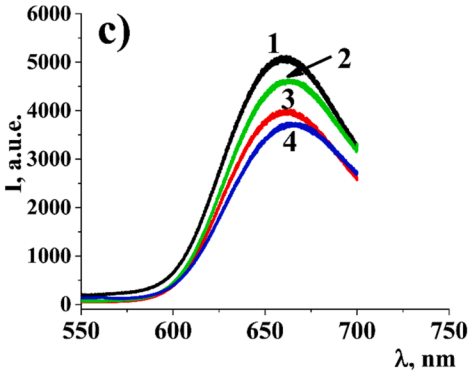

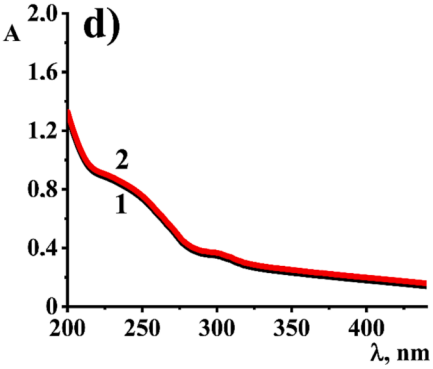

Fig. 4. (a)The release of NO measured by the Griess reagent-analysis for **1**, **2** or **3** complexes (1–3), **1**(**2** or **3**)@SNs-NH_2 (4–6) and for **1**(**2** or **3**)@SNs-NH_2-{Mo_6I_8} (7–9). (b) Electrochemical potentials of complexes **1**–**3** and **1**(**2** or **3**)@SNs-NH_2. Modified glassy carbon electrode, CH_3CN/Bu_4NBF_4. E_p, V ref. $Ag/AgNO_3$. (c) Emission spectra of [{Mo_6I_8}$(CH_3COO)_6$]$^{2-}$ (0.035 mM) in aqueous solution (1), aqueous colloids (0.5 g•L^{-1}): **1**@SNs-NH_2-{Mo_6I_8} (2), **2**@SNs-NH_2-{Mo_6I_8} (3), **3**@SNs-NH_2-{Mo_6I_8} (4); λ_{ex} = 380 nm. (d) UV–visible spectra of aqueous dispersions of (**1**)@SN-NH_2–{Mo_6I_8} before (1) and after 1 h of irradiation (2) (405 nm).

observed for **1**(**2** or **3**)@SNs-NH_2, although some change in the potentials (Fig. 4b) *vs* the initial complexes can be explained by the influence of silica matrix as the new environment of the complex. The presence of the first and second reductive waves is discussed in literature as the formal reduction of the nitrosyl ligand from NO^+ to NO·, and the second wave represents further reduction to NO^- [57,58]. However, both vigorous gas evolution and irreversibility of electron transfer at first stage (E_p^1) argue for the fact that the first reductive wave is followed by the rapid subsequent NO evolution. Thus, we assume that the second reduction peak is metal-centered, given that the ligands of the complex are not redox active.

Thus, reduction processes, including those arisen from the intracellular glutathione level [16], can favor the NO release even in the absence of light irradiation.

3.3. Synthesis of heterometallic nanocomposites and their photo-induced transformations

Both positively charged surface and the great number of the surface exposed amino-groups make **1**(**2** or **3**)@SNs-NH_2 nanoparticles good basis for the deposition of [{Mo_6I_8}$(CH_3COO)_6$]$^{2-}$ cluster units. The deposition of the cluster units onto **1**(**2** or **3**)@SNs-NH_2 was performed through the previously published technique [12] based on the treating of the nanoparticles in the aqueous solution of [{Mo_6I_8}$(CH_3COO)_6$]$^{2-}$ (**{Mo_6I_8}**) with further phase separation in the specific conditions (Fig. 1a; for the details see the Exp. Section). The luminescence analysis of the separated colloids and supernatants reveals the transfer of the luminescent cluster units from the aqueous solutions to the separated colloids. The deposition of the cluster onto **1**(**2** or **3**)@SNs-NH_2 is manifested by the appearance of the emissive band peculiar for {Mo_6I_8} (Fig. 4c). It is worth noting that the ligand exchange is possible in the aqueous solutions of [{Mo_6I_8}$(CH_3COO)_6$]$^{2-}$, and some of apical positions can be aquated under their deposition onto the SNs. Thus, herein and further the cluster units will be designated as [{Mo_6I_8}L_6]$^{2-}$ or {Mo_6I_8}. The surface charge neutralization followed by the enhanced aggregation of the composite SNs (Table 1) provides one more evidence of the adsorption of {Mo_6I_8} onto **1**(**2** or **3**)@SNs-NH_2 with the formation of **1**(**2** or **3**)@SNs-NH_2-{Mo_6I_8}. The Si:Ru molar ratios calculated from the data of ICP-OES method are collected in Table 1, while the EDX analysis of the dried samples of **1**(**2** or **3**)@SNs-NH_2-{Mo_6I_8} confirms the combination of Ru and Mo in the SNs (Fig. S6).

The high aggregation of **1**(**2** or **3**)@SNs-NH_2-{Mo_6I_8} can restrict their ability to be taken by cells. However, the protein corona formation can affect both aggregation and cellular uptake behavior of nanoparticles [59]. Indeed, the aggregation of **1**(**2** or **3**)@SNs-NH_2-{Mo_6I_8} colloids is significantly decreased after their treating with BSA (Table 1). The treating was performed through the centrifugation and washing steps in order to wash out the residual amounts of BSA. Thus, the observed negative electrokinetic potential values derives from the well-known protein corona.

The poor irradiation-induced spectral changes of **1**(**2** or **3**)@SNs-NH_2-{Mo_6I_8} are similar with those of **1**(**2** or **3**)@SNs-NH_2 (Fig. 4d, Fig. S7). The Griess analysis confirms the aforesaid tendency (Fig. 4a).

Hexamolybdenum cluster complexes with specific structure are promising basis for efficient ROS-generation [60]. It has been previously reported that the deposition of the similar cluster units onto amino-modified SNs results in SNs-NH_2-{Mo_6I_8}, which exhibit high level of ROS generation and high photodynamic activity manifested by the photo-induced cell death [12,61]. However, the poor level of the generated ROS in the aqueous dispersions of **1**(**2** or **3**)@SNs-NH_2-{Mo_6I_8} (Fig. S8) can be explained by the inner-filter effect arisen from the absorptivity of **1**(**2** or **3**)@SNs-NH_2.

3.4. Release of the complexes from *1*(*2* or *3*)@SNs-NH_2 and *1*(*2* or *3*)@SNs-NH_2-{Mo_6I_8}

The insignificant responsivity of the composite SNs to the irradiation is a prerequisite for very poor if any irradiation-induced cytotoxicity. However, the analysis of cytotoxicity of **1**(**2** or **3**)@SNs-NH_2 and **1**(**2** or **3**)@SNs-NH_2-{Mo_6I_8} should be preceded by the analysis of the release of both Ru^{II} nitrosyl and {Mo_6I_8} cluster complexes from the SNs. The ICP-OES analysis allows the quantitative comparison of Si:Ru molar ratios before and after continuous stirring of **1**(**2** or **3**)@SNs-NH_2 in the buffered solutions (Table 2) with the following appearance of the

Table 2
ICP-OES data for **1**(**2** or **3**)@SNs-NH_2 and **1**(**2** or **3**)@SNs-NH_2-$\{Mo_6I_8\}$ after treatment by phosphate buffer (pH 6.8) and acetate buffer (pH 4.5) (see details in Exp. section).

Sample	Si:Ru:Mo
1@SNs-NH_2 pH 6.8	1:0.010
2@SNs-NH_2 pH 6.8	1:0.010
3@SNs-NH_2 pH 6.8	1:0.010
1@SNs-NH_2-$\{Mo_6I_8\}$ pH 6.8	1:0.013:0.010
2@SNs-NH_2-$\{Mo_6I_8\}$ pH 6.8	1:0.014:0.005
3@SNs-NH_2-$\{Mo_6I_8\}$ pH 6.8	1:0.012:0.006
1@SNs-NH_2-$\{Mo_6I_8\}$ pH 4.5	1:0.011:0.002
2@SNs-NH_2-$\{Mo_6I_8\}$ pH 4.5	1:0.010:0.004
3@SNs-NH_2-$\{Mo_6I_8\}$ pH 4.5	1:0.010:0.001

ruthenium complexes in the supernatants (Table S2). The leaching is about 40%, although the IR analysis of the dried samples of **1**(**2** or **3**)@SNs-NH_2 after the leaching still remains the presence of nitrosyls (Fig. S9). Thus, the leaching predominantly occurs for the complexes undergone the nitrosyl-nitro transformation *via* the equilibrium (1), while the Ru^{II} nitrosyl complexes located in the interior of the SNs exhibit the low tendency to leaching.

The specificity of cytoplasmic and lysosomal conditions of tumor cells can create a favorable environment for reduction processes, which favors NO release from Ru^{II} nitrosyl complexes [16]. Thus, the lysosomal environment was modeled by the acidification to pH 4.5, however, the initial complexes remain unchanged in the acidified solutions (Fig. S9). The aforesaid excludes specific transformations of the complexes in the lysosomal environment as a driving force for a release of NO. No detectable enhancement of the leaching extent is observed for **1**(**2** or **3**)@SNs-NH_2 in either acidified (Fig. S10 a-c) or GSH neutral solutions (Table S3).

The UV–Vis spectra of the supernatants after the continuous stirring of **1**(**2** or **3**)@SNs-NH_2-$\{Mo_6I_8\}$ in neutral solutions and further phase separation indicate the lower intensity bands than in the case of **1**(**2** or **3**)@SNs-NH_2 (Fig. S10 a-c). This agrees well with the ICP-OES analysis of the heterometallic SNs after the stirring at pH 6.8 (Table 2), thus, indicating that the exterior deposition of $\{Mo_6I_8\}$ restricts the leaching of the ruthenium complexes. The leaching of the cluster units becomes greater under their stirring in the acidified solutions, which is evident from both increased intensity of the UV–Vis bands in the supernatants (Fig. S10 d-f) and the Si:Ru:Mo ratios evaluated by the ICP-OES method (Table 2). This allows to explain the leaching of the cluster units by the production of the neutral cluster form $[\{Mo_6I_8\}L_4(H_2O)_2]$, in turn, arisen from the aquation of the apical positions through the equilibrium (3) [62].

$$[\{Mo_6I_8\}L_6]^{2-} + 2H^+ + 2H_2O = [\{Mo_6I_8\}L_4(H_2O)_2] + 2HL \quad (3)$$

3.5. *"Dark" and photo-induced cytotoxicity of the complexes and the SNs*

The incubation of the cell samples of cancer (M-HeLa) and normal (Chang Liver) cell lines with complexes **1**–**3** induces poor effect on the cell viability in both "dark" and light irradiation conditions (Fig. 5 a-c, Table S4, Fig. S11). The similar effects are observed after the incubation of the cell samples with **1**(**2** or **3**)@SNs (Fig. 5 a-c, Fig. S11). This can be explained by the poor cell internalization of the initial complexes and their negatively charged nanoparticulate forms. The cell viability results reveal the similar effect of the complexes and their nanoparticulate forms on M-HeLa and Chang Liver cell lines (Fig. 5 a-c, Table S4, Fig. S11), thus, the comparative analysis of the different nanoparticulate forms is represented for M-HeLa cell line.

The amino-modified counterparts of the aforesaid nanocomposites (**1**(**2** or **3**)@SNs-NH_2) demonstrate greater "dark" cytotoxicity than that of **1**(**2** or **3**)@SNs, which is demonstrated in Fig. 5a-c by plotting of the cell viability *vs* concentrations of complexes **1**–**3** in both initial molecular and the nanoparticulate forms. The results (Fig. 5a-c) correlates with the well-known tendency that the embedding of amino-groups onto the surfaces of the SNs increases their cell internalization [27,29]. The cell viability values of both **1**(**2** or **3**)@SNs and **1**(**2** or **3**)@SNs-NH_2 do not reach IC_{50} in the studied concentration range (Fig. 5). However, the effect of the SNs on the cell viability is greater than that of the complexes in aqueous solutions (Fig. 5 a-c). The significant increase in the cytotoxicity of **1**(**2** or **3**)@SNs-NH_2-$\{Mo_6I_8\}$ *vs* **1**(**2** or **3**)@SNs-NH_2 looks rather unexpected, since the previously published work [61] reveals the low cytotoxicity of amino-modified silica nanoparticles deposited with $\{Mo_6I_8\}$. The cell viability data of **1**(**2** or **3**)@SNs-NH_2-$\{Mo_6I_8\}$ allow the determination of the IC_{50} values, which are represented in Table included into Fig. 5.

The red emission of the cluster units allows to evaluate the cell internalization and intracellular trafficking of **1**(**2** or **3**)@SNs-NH_2-$\{Mo_6I_8\}$ by flow cytometry and fluorescent microscopy measurements (Figs. 5, 6, S12). The efficient cell marking demonstrated by the confocal microscopy images (Fig. 5 d) correlates with the high level of the cell internalization (Fig. 6 a, b). The internalized heterometallic SNs localize in cell cytoplasm with the detectable entering the cell nuclei as it is visualized by the confocal microscopy images (Fig. 5d).

The efficient cell internalization of **1**(**2** or **3**)@SNs-NH_2-$\{Mo_6I_8\}$ disagrees with their high aggregation in aqueous dispersions (Table 1). However, it agrees well with the aggregation behavior of the colloids treated with BSA (Table 1). Thus, the presence of BSA in the nutrient media applied for the incubation of the cell samples with the SNs can be considered as the factor facilitating their cell internalization due to the formation of the protein corona.

The cell viability of M-HeLa cells incubated with **1**(**2** or **3**)@SNs-NH_2 decreases to 20% after the irradiation for 30 min (Fig. S11), while the photo-effect on the cell viability is on the same level or even smaller for **1**(**2** or **3**)@SNs-NH_2-$\{Mo_6I_8\}$. This fact agrees well with the above mentioned tendency that the incorporation of both Ru^{II} nitrosyl and $\{Mo_6I_8\}$ complexes into **1**(**2** or **3**)@SNs-NH_2-$\{Mo_6I_8\}$ significantly suppress their photochemical and photodynamic activities. The low level of the photo-induced cytotoxicity disagrees with the significant leaching of the complexes from **1**(**2** or **3**)@SNs-NH_2 (Table 2, Table S2). However, this agrees well with the above mentioned tendency that the leaching predominantly occurs for the complexes undergone the nitrosyl-nitro transformation, while the photochemically active Ru^{II} nitrosyl complexes exhibit the low tendency to leaching.

The release of protons following the nitrosyl-nitro transformation *via* the equilibrium (1) can trigger the back nitro-nitrosyl transformation of the complexes located at the exterior of **1**(**2** or **3**)@SNs-NH_2. However, the basicity of the surface exposed amino-groups prerequisites the binding of the released protons as it is schematically illustrated in Fig. 6c. The extra-protonation of the amino-groups provides a reason for enhancing both adsorption of $\{Mo_6I_8\}$ cluster units onto **1**(**2** or **3**)@SNs-NH_2 and their aquation through the equilibrium (3). It is worth noting that commonly reported low cytotoxicities of $\{Mo_6I_8\}$ clusters derive from either low cell internalization [63] or insignificant leaching of the cluster units from the nanocomposites [12,61]. This allows to correlate the observed high cytotoxicity of **1**(**2** or **3**)@SNs-NH_2-$\{Mo_6I_8\}$ with the leaching of the $\{Mo_6I_8\}$ units undergone the aquation. As it was previously demonstrated [62] the aquated cluster units tend to form the aggregates, which exhibit the pronounced cytotoxicity.

4. Conclusion

In summary, Ru^{II} nitrosyl complexes ($[Ru(NO)(NH_3)_2Py_2(NO_3)](NO_3)_2$, $[Ru(NO)(NH_3)_4OH]Cl_2$ and $[Ru(NO)Py_4OH](PF_6)_2$) exhibiting photo- and redox-induced release of NO in aqueous solutions are introduced as metal complex blocks for incorporation into interior zone of amino-modified silica nanoparticles (SNs). The spectral profiles of the incorporated Ru^{II} nitrosyl complexes differ from those of the initial

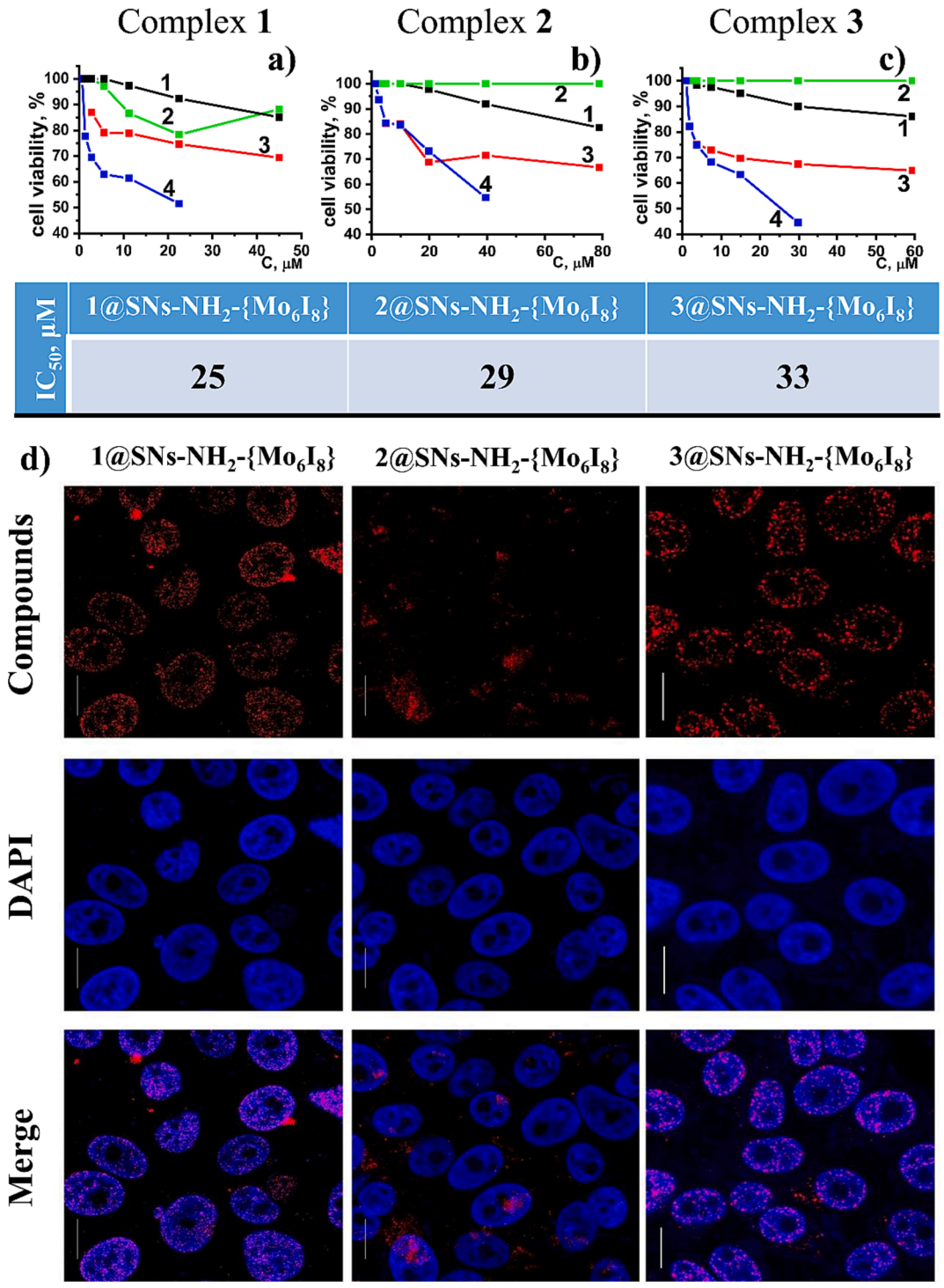

Fig. 5. (a-c) Cell viability of M-HeLa incubated by various concentrations of complexes **1** (a), **2** (b) and **3** (c) in both molecular and nanoparticulate forms: 1 (black) – molecular complex, 2 (green) – **1**(**2** or **3**)@SNs, 3 (red) – **1**(**2** or **3**)@SNs-NH_2, 4 (blue) – **1**(**2** or **3**)@SNs-NH_2-$\{Mo_6I_8\}$. (d) Confocal microscopy images of M-HeLa cells after 24 h incubation with **1**(**2** or **3**)@SNs-NH_2-$\{Mo_6I_8\}$ (0.12 g•L^{-1}); scale bar 20 μm. IC_{50} values for **1**(**2** or **3**)@SN-NH_2-$\{Mo_6I_8\}$ are represented in the Table.

complexes in the aqueous solutions due to the ligand exchange processes, including those arisen from nitrosyl-nitro transformation. The latter transformation is followed by the release of protons, which enhances the conversion of the surface exposed amino-groups into the ammonium-groups followed by the increase in the positive charging of the amino-modified Ru^{II}-doped SNs. The IR spectra of the SNs reveal the Ru^{II} nitrosyl complexes, but their interior localization suppresses their ability to photo-induced release of NO. The surface decoration of the Ru^{II}-doped SNs by amino-groups enhances their cell internalization. This along with the leaching extent of the ruthenium complexes from the SNs explains the greater suppression of the cell viability in comparison with the initial complexes.

The exterior deposition of $\{Mo_6I_8\}$-cluster units onto the SNs doped with Ru^{II} nitrosyl complexes is represented as a route to synthesize heterometallic SNs. The combination of the two photo-active components as Ru^{II} nitrosyl and $\{Mo_6I_8\}$-based cluster complexes in the SNs results in the antisynergistic effect on their photochemical and photodynamical properties. The red emission of the heterometallic SNs arisen

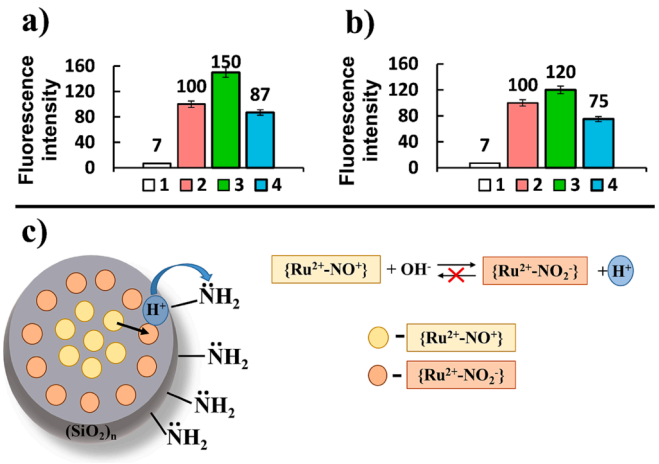

Fig. 6. (a, b) Study of cellular uptake of **1**(**2** or **3**)@SNs-NH_2-{Mo_6I_8} (0.25 g•L^{-1}) by M-HeLa cells (a) and Chang Liver cells (b): Control (1); **1**@SNs-NH_2-{Mo_6I_8} (2); **2**@SNs-NH_2-{Mo_6I_8} (3); **3**@SNs-NH_2-{Mo_6I_8} (4). (c) The schematic illustration of how the surface exposed amino-groups capture the protons released due to nitrosyl-nitro transformations of the complexes inside **1**(**2** or **3**)@SNs-NH_2.

from the luminescent {Mo_6I_8}-clusters allows the visualization of the efficient cell internalization of the SNs. The low photo-activities of the both components explain the low photo-induced cytotoxicity of the heterometallic SNs.

The red emission of the cluster units reveals the efficient cell internalization of the heterometallic SNs followed by their distribution within the cell cytoplasm and entering the cell nuclei. It is also demonstrated that the presence of BSA in the nutrient media applied in the incubation of the cell samples by the heterometallic SNs facilitates their cell internalization through the protein corona formation.

The so-called dark cytotoxicity measurements reveal the synergistic effect of the components, which correlates with the detectable leaching of {Mo_6I_8}-clusters from the heterometallic SNs at pH 6.8. This allows to propose that the exterior Ru^{II} complexes and their transformations can be a factor facilitating the leaching of the {Mo_6I_8}-clusters.

Funding

This research did not receive any specific grant from funding agencies in the public, commercial, or not-for-profit sectors.

CRediT authorship contribution statement

Olga Bochkova: Writing – original draft, Visualization, Investigation. **Svetlana Fedorenko:** Writing – original draft, Investigation. **Artem Mikhailov:** Resources, Investigation. **Gennadiy Kostin:** Resources. **Maxim Mikhailov:** Investigation. **Maxim Sokolov:** Investigation. **Julia Elistratova:** Investigation. **Kirill Kholin:** Investigation. **Maxim Tarasov:** Investigation. **Yulia Budnikova:** Investigation. **Guzel Sibgatullina:** Investigation. **Dmitry Samigullin:** Investigation. **Irek Nizameev:** Investigation. **Vadim Salnikov:** Investigation. **Ivan Yakovlev:** Investigation. **Darina Rozhentsova:** Investigation. **Anna Lyubina:** Investigation. **Syumbelya Amerhanova:** Investigation. **Alexandra Voloshina:** Investigation. **Tatiana Gerasimova:** Investigation. **Asiya Mustafina:** Writing – review & editing, Supervision, Conceptualization.

Declaration of Competing Interest

The authors declare that they have no known competing financial interests or personal relationships that could have appeared to influence the work reported in this paper.

Data availability

Data will be made available on request.

Acknowledgements

Authors gratefully acknowledge to Assigned Spectral-Analytical Center of FRC Kazan Scientific Center of RAS for providing necessary facilities to carry out physical-chemical measurements. The authors thanks to Interdisciplinary Center for Analytical Microscopy at KFU for assistance with the confocal microscopy experiments.

Appendix A. Supplementary data

Supplementary data to this article can be found online at https://doi.org/10.1016/j.jphotochem.2023.115147.

References.

[1] M.J. Son, T. Kim, S.W. Lee, Facile synthesis of fluorescent mesoporous nanocarriers with pH-sensitive controlled release of naturally derived dieckol, Colloids Surf., A 657 (2023), 130535, https://doi.org/10.1016/j.colsurfa.2022.130535.
[2] J. Zhuang, Y. Yu, R. Lu, Mesoporous silica nanoparticles as carrier to overcome bacterial drug resistant barriers, Int. J. Pharm. 631 (2022), 122529, https://doi.org/10.1016/j.ijpharm.2022.122529.
[3] N. Ghosh, M. Kundu, S. Ghosh, A.K. Das, S. De, J. Das, P.C. Sil, pH-responsive and targeted delivery of chrysin via folic acid-functionalized mesoporous silica nanocarrier for breast cancer therapy, Int. J. Pharm. 631 (2023), 122555, https://doi.org/10.1016/j.ijpharm.2022.122555.
[4] Y. Romdoni, G.T. Kadja, Y. Kitamoto, M. Khalil, Synthesis of multifunctional Fe3O4@ SiO2-Ag nanocomposite for antibacterial and anticancer drug delivery, Appl. Surf. Sci. 610 (2023), 155610, https://doi.org/10.1016/j.apsusc.2022.155610.
[5] A. Abulikemu, X. Zhao, H. Xu, Y. Li, R. Ma, Q. Yao, C. Guo, Silica nanoparticles aggravated the metabolic associated fatty liver disease through disturbed amino acid and lipid metabolisms-mediated oxidative stress, Redox Biol. 59 (2023), 102569, https://doi.org/10.1016/j.redox.2022.102569.
[6] G. Zhou, J. Wang, L. Ren, J. Liu, X. Li, Y. Zhang, X. Zhou, Silica nanoparticles suppressed the spermatogenesis via downregulation of miR-450b-3p by targeting Layilin in spermatocyte of mouse, Environ. Pollut. 318 (2023), 120864, https://doi.org/10.1016/j.envpol.2022.120864.
[7] Z. Zhang, W. Li, D.i. Chang, Z. Wei, E. Wang, J. Yu, Y. Xu, Y. Que, Y. Chen, C. Fan, B. Ma, Y. Zhou, Z. Huan, C. Yang, F. Guo, J. Chang, A combination therapy for androgenic alopecia based on quercetin and zinc/copper dual-doped mesoporous silica nanocomposite microneedle patch, Bioact. Mater. 24 (2023) 81–95.
[8] W. Wei, M. Wei, S. Liu, Silica nanoparticles as a carrier for signal amplification, Rev. Anal. Chem 31 (2012) 163–176, https://doi.org/10.1515/revac-2012-0021.
[9] L. Kou, J. Sun, Y. Zhai, Z. He, The endocytosis and intracellular fate of nanomedicines: Implication for rational design, Asian, J. Pharm. Sci. 8 (2013) 1–10, https://doi.org/10.1016/j.ajps.2013.07.001.
[10] P.H. Hemmerich, A.H. von Mikecz, B. Xu, Defining the subcellular interface of nanoparticles by live-cell imaging, PLoS One 8 (4) (2013) e62018.
[11] Y. Chen, Q. Yin, X. Ji, S. Zhang, H. Chen, Y. Zheng, Y. Sun, H. Qu, Z. Wang, Y. Li, X. Wang, K. Zhang, L. Zhang, J. Shi, Manganese oxide-based multifunctionalized mesoporous silica nanoparticles for pH-responsive MRI, ultrasonography and circumvention of MDR in cancer cells, Biomaterials 33 (2012) 7126–7137, https://doi.org/10.1016/j.biomaterials.2012.06.059.
[12] E. Fanizza, R. Mastrogiacomo, O. Pugliese, A. Guglielmelli, L. De Sio, R. Castaldo, N. Depalo, NIR-absorbing mesoporous silica-coated copper sulphide nanostructures for light-to-thermal energy conversion, Nanomaterials 12 (2022) 2545, https://doi.org/10.3390/nano12152545.
[13] J. Elistratova, A. Mukhametshina, K. Kholin, I. Nizameev, M. Mikhailov, M. Sokolov, R. Khairullin, R. Miftakhova, G.h. Shammas, M. Kadirov, K. Petrov, A. Rizvanov, A. Mustafina, Interfacial uploading of luminescent hexamolybdenum cluster units onto amino-decorated silica nanoparticles as new design of nanomaterial for cellular imaging and photodynamic therapy, J. Colloid Interface Sci. 538 (2019) 387–396, https://doi.org/10.1016/j.jcis.2018.12.013.
[14] I. Stepanenko, M. Zalibera, D. Schaniel, J. Telser, V.B. Arion, Ruthenium-nitrosyl complexes as NO-releasing molecules, potential anticancer drugs, and photoswitches based on linkage isomerism, Dalton Trans. 51 (2022) 5367–5393, https://doi.org/10.1039/d2dt00290f.
[15] L. Xu, Z. Ma, W. Wang, L. Xie, L. Liu, J. Liu, X. Zhao, H. Wang, Photo-induced cytotoxicity, photo-controlled nitric oxide release and DNA/human serum albumin binding of three water-soluble nitrosylruthenium complexes, Polyhedron 137 (2017) 157–164.
[16] C.F.N. da Silva, B. Possato, L.P. Franco, L.C.B. Ramos, S. Nikolaou, The role of ancillary ligand substituents in the biological activity of triruthenium-NO complexes, J. Inorg. Biochem. 186 (2018) 197–205, https://doi.org/10.1016/j.jinorgbio.2018.05.021.

[17] R.P. Orenha, G.C.G. Silva, A.P. de Lima Batista, A.G.S. de Oliveira Filho, N. H. Morgon, V.B. da Silva, S.S.P. Furtado, G.F. Caramori, M.J. Piotrowski, R.L. T. Parreira, Tracking the role of trans-ligands in ruthenium–NO bond lability: computational insight, New J. Chem. 44 (27) (2020) 11448–11456.
[18] A.P. Gaspari, R.S. da Silva, Z.A. Carneiro, M.R. de Carvalho, I. Carvalho, L. Pernomian, L.P. Ferreira, L.C.B. Ramos, G.A. de Souza, A.L. Formiga, Improving cytotoxicity against breast cancer cells by using mixed-ligand ruthenium (II) complexes of 2, 2'-bipyridine, amino acid, and nitric oxide derivatives as potential anticancer agents, Anticancer Agents Med Chem. 21 (2021) 1602–1611, https://doi.org/10.2174/1871520621666210120155105.
[19] R.P. Orenha, G.C.G. Silva, N.H. Morgon, G.F. Caramori, R.L.T. Parreira, Can the relative positions (cis–trans) of ligands really modulate the coordination of NO in ruthenium nitrosyl complexes? New J. Chem. 45 (2021) 1658–1666, https://doi.org/10.1039/d0nj05262k.
[20] E. D. Stolyarova, A. A. Mikhailov, A. A. Ulantikov, J. A. Eremina, L. S. Klyushova, N. V. Kuratieva, V.A. Nadolinny, G. A. Kostin, Blue-to-red light triggered nitric oxide release in cytotoxic/cytostatic ruthenium nitrosyl complexes bearing biomimetic ligands, J. Photochem. Photobiol., A 421 (2021) 113520, doi:10.1016/j.jphotochem.2021.113520.
[21] I.A. Yakovlev, A.A. Mikhailov, J.A. Eremina, L.S. Klyushova, V.A. Nadolinny, G. A. Kostin, Nitric oxide release and related light-induced cytotoxicity of ruthenium nitrosyls with coordinated nicotinate derivatives, Dalton Trans. 50 (2021) 13516–13527, https://doi.org/10.1039/d1dt02190g.
[22] I.S. Fomenko, A.A. Mikhailov, V. Vorobyev, N.V. Kuratieva, G.A. Kostin, D. Schaniel, V.A. Nadolinny, A.L. Gushchin, Solution and solid-state light-induced transformations in heterometallic vanadium-ruthenium nitrosyl complex, J. Photochem. Photobiol., A 407 (2021), 113044, https://doi.org/10.1016/j.jphotochem.2020.113044.
[23] N. Sharma, V. Kumar, D.A. Jose, A ruthenium nitrosyl complex-based highly selective colorimetric sensor for biological H_2S and H_2S–NO cross-talk regulated release of NO, Dalton Trans. 52 (2023) 675–682, https://doi.org/10.1039/D2DT03108F.
[24] P. Labra-Vázquez, M. Bocé, M. Tassé, S. Mallet-Ladeira, P.G. Lacroix, N. Farfán, I. Malfant, Chemical and photochemical behavior of ruthenium nitrosyl complexes with terpyridine ligands in aqueous media, Dalton Trans. 49 (2020) 3138–3154, https://doi.org/10.1039/C9DT04832D.
[25] R.P. Orenha, N.H. Morgon, J. Contreras-García, G.C.G. Silva, G.R. Nagurniak, M. J. Piotrowski, G.F. Caramori, A. Muñoz-Castro, R.L.T. Parreira, How does the acidic milieu interfere in the capability of ruthenium nitrosyl complexes to release nitric oxide? New J. Chem. 44 (2020) 773–779, https://doi.org/10.1039/c9nj04643g.
[26] B. Giri, T. Saini, S. Kumbhakar, K. Selvan, A. Muley, A. Misra, S. Maji, Near-IR light-induced photorelease of nitric oxide (NO) on ruthenium nitrosyl complexes: formation, reactivity, and biological effects, Dalton Trans. 49 (2020) 10772–10785, https://doi.org/10.1039/d0dt01788d.
[27] N. Sharma, P. Arjunan, S. Marepally, N. Jain, A. R. Naziruddin, A. Ghosh, C. R. Mariappan, D.A. Jose, Photo controlled release of nitric oxide (NO) from amphiphilic and nanoscale vesicles based ruthenium nitrosyl complex: NO release and cytotoxicity studies, J. Photochem. Photobiol., A, 425 (2021) 113703, doi: 10.1016/j.jphotochem.2021.113703.
[28] N. Sharma, D.A. Jose, N. Jain, S.h. Parmar, A. Srivastav, J. Chawla, A. R. Naziruddin, C.R. Mariappan, Regulation of Nitric Oxide (NO) Release by Membrane Fluidity in Ruthenium Nitrosyl Complex-Embedded Phospholipid Vesicles, Langmuir 38 (2022) 13602–13612, https://doi.org/10.1021/acs.langmuir.2c02457.
[29] L. Song, L. Xie, L. Xu, Q.i. Jing, C. Liu, X. Xi, W. Wang, Y.i. Zhao, X. Zhao, H. Wang, Syntheses, spectra, photoinduced nitric oxide release and interactions with biomacromolecules of three nitrosylruthenium complexes, Polyhedron 185 (2020) 114596.
[30] M. L. M. do Amaral, R. D. Nascimento, L. F. Silva, E. C. de Souza Arantes, A. E. Graminha, R. S. da Silva, R. G. de Lima, New trans-[Ru (NO)(NO2)(dppb)(o-bdqi)] + complex as NO donor encapsulated Pluronic F-127 micelles, Polyhedron 218 (2022) 115770, doi.org/10.1016/j.poly.2022.115770.
[31] F.G. Doro, U.P. Rodrigues-Filho, E. Tfouni, A regenerable ruthenium tetraammine nitrosyl complex immobilized on a modified silica gel surface: Preparation and studies of nitric oxide release and nitrite-to-NO conversion, J. Colloid Interface Sci. 307 (2007) 405–417, https://doi.org/10.1016/j.jcis.2006.11.013.
[32] R. Galvão de Lima, M.G. Sauaia, C. Ferezin, I.M. Pepe, N.M. José, L.M. Bendhack, Z. Novais da Rocha, R. Santana da Silva, Photochemical and pharmacological aspects of nitric oxide release from some nitrosyl ruthenium complexes entrapped in sol–gel and silicone matrices, Polyhedron 26 (2007) 4620–4624, https://doi.org/10.1016/j.poly.2007.03.042.
[33] A.A. Eroy-Reveles, Y. Leung, P.K. Mascharak, Release of Nitric Oxide from a Sol−Gel Hybrid Material Containing a Photoactive Manganese Nitrosyl upon Illumination with Visible Light, J. Am. Chem. Soc. 128 (2006) 7166–7167, https://doi.org/10.1021/ja061852n.
[34] N.D. Donahue, H. Acar, St. Wilhelm, Concepts of nanoparticle cellular uptake, intracellular trafficking, and kinetics in nanomedicine, Adv. Drug Deliv. Rev. 143 (2019) 68–96, https://doi.org/10.1016/j.addr.2019.04.008.
[35] D. Manzanares, V. Ceña, Endocytosis: the nanoparticle and submicron nanocompounds gateway into the cell, Pharmaceutics 12 (2020) 371, https://doi.org/10.3390/pharmaceutics12040371.
[36] E. Tfouni, D.R. Truzzi, A. Tavares, A.J. Gomes, L.E. Figueiredo, D.W. Franco, Biological activity of ruthenium nitrosyl complexes, Nitric Oxide 26 (2012) 38–53, https://doi.org/10.1016/j.niox.2011.11.005.
[37] R.M. Carlos, A.A. Ferro, H.A.S. Silva, M.G. Gomes, S.S.S. Borges, P.C. Ford, E. Tfouni, D.W. Franco, Photochemical reactions of trans-[Ru (NH3) 4L (NO)] 3+ complexes, Inorg. Chim. Acta 357 (5) (2004) 1381–1388.
[38] V. Vorobyev, G.A. Kostin, I.A. Baidina, A.A. Mikhailov, I.V. Korolkov, V. A. Emelyanov, Synthesis of the ruthenium nitrosyl complex with coordinated ammonia and pyridine at room temperature, Z. Anorg. Allg. Chem. 646 (2020) 58–64, https://doi.org/10.1002/zaac.201900246.
[39] M.A. Il'yin, V.A. Emel'anov, A.V. Belyaev, A.N. Makhinya, S.V. Tkachev, N. I. Alferova, New method for the synthesis of trans-hydroxotetraamminenitrosoruthenium(II) dichloride and its characterization, Russ. J. Inorg. Chem. 53 (7) (2008) 1070–1076.
[40] A.A. Mikhailov, G.A. Kostin, D. Schaniel, The influence of the *trans*-ligand to NO on the thermal stability of the photoinduced side-bond coordinated linkage isomer, New J. Chem. 46 (2022) 12641–12650, https://doi.org/10.1039/D2NJ01388F.
[41] M.A. Mikhailov, K.A. Brylev, P.A. Abramov, E. Sakuda, S. Akagi, A. Ito, N. Kitamura, M.N. Sokolov, Core cluster complexes by terminal carboxylate ligands, Inorg. Chem. 55 (2016) 8437–8445, https://doi.org/10.1021/acs.inorgchem.6b01042.
[42] Y. Chen, Y. Zhang, Fluorescent quantification of amino groups on silica nanoparticle surfaces, Anal. Bioanal. Chem. 399 (2011) 2503–2509, https://doi.org/10.1007/s00216-010-4622-7.
[43] R.R. Sharipova, M.G. Belenok, B.F. Garifullin, A.S. Sapunova, A.D. Voloshina, O. V. Andreeva, I.Y. Strobykina, P.V. Skvortsova, Y.F. Zuev, V.E. Kataev, Synthesis and anti-cancer activities of glycosides and glycoconjugates of diterpenoid isosteviol, Med Chem Comm. 10 (2019) 1488–1498, https://doi.org/10.1039/C9MD00242A.
[44] M.B. Fairy, R.J. Irving, Complexes of ruthenium nitrosyl trihalides, J. Chem. Soc. A (1966) 475–479, https://doi.org/10.1039/J19660000475.
[45] M.J. Rose, P.K. Mascharak, Photoactive ruthenium nitrosyls: Effects of light and potential application as NO donors, Coordin, Chem. Rev. 252 (2008) 2093–2114, https://doi.org/10.1016/j.ccr.2007.11.011.
[46] T.J. Meyer, J.B. Godwin, N. Winterton, The reversible conversion of co-ordinated nitrosyl into co-ordinated nitrite in 2,2′-bipyridyl complexes of ruthenium(II), J. Chem. Soc. D 14 (1970) 872, https://doi.org/10.1039/C29700000872.
[47] J.B. Godwin, T.J. Meyer, Nitrosyl-nitrite interconversion in ruthenium complexes, Inorg. Chem. 10 (1971) 2150–2153, https://doi.org/10.1021/ic50104a012.
[48] S. Fedorenko, A. Stepanov, O. Bochkova, K. Kholin, I. Nizameev, A. Voloshina, O. Tyapkina, D. Samigullin, S. Kleshnina, B. Akhmadeev, A. Romashchenko, E. Zavjalov, R. Amirov, A. Mustafina, Specific nanoarchitecture of silica nanoparticles codoped with the oppositely charged Mn2+ and Ru2+ complexes for dual paramagnetic-luminescent contrasting effects, Nanomed. – Nanotechnol., 49 (2023) 102665, doi.org/10.1016/j.nano.2023.102665.
[49] L. Bergman, J. Rosenholm, A.-B. Öst, A. Duchanoy, P. Kankaanpaa, J. Heino, M. Linden, On the complexity of Electrostatic suspension stabilization of functionalized silica nanoparticles for biotargeting and imaging application, J. Nanomater. (2008) Article ID 712514, doi: 10.1155/2008/712514.
[50] N. Davydov, A. Mustafina, V. Burilov, E. Zvereva, S. Katsyuba, L. Vagapova, A. Konovalov, I. Antipin, Complex formation of d-metal ions at the interface of TbIII-doped silica nanoparticles as a basis of substrate-responsive TbIII-centered luminescence, ChemPhysChem 13 (2012) 3357–3364, https://doi.org/10.1002/cphc.201200367.
[51] P. Labra-Vázquez, M. Boce, M. Tassé, S. Mallet-Ladeira, P.G. Lacroix, N. Farfan, I. Malfant, Chemical and photochemical behavior of ruthenium nitrosyl complexes with terpyridine ligands in aqueous media, Dalton Trans. 49 (2020) 3138–3154, https://doi.org/10.1039/C9DT04832D.
[52] A.A. Mikhailov, V.A. Vorobyev, V.A. Nadolinny, Y.V. Patrushev, Y.S. Yudina, G. A. Kostin, Primary and secondary photochemical transformations of biologically active precursor-Nitro-Nitrosyl ruthenium complex, J. Photochem. Photobio. A 373 (2019) 37–44, https://doi.org/10.1016/j.jphotochem.2018.12.037.
[53] A. Chakraborty, N. Gupta, K. Ghosh, P. Roy, In vitro evaluation of the cytotoxic, anti-proliferative and anti-oxidant properties of pterostilbene isolated from Pterocarpus marsupium, Toxicol. In Vitro 24 (2010) 1215–1228, https://doi.org/10.1016/j.tiv.2010.02.007.
[54] D. Zhang, Z. Wu, J. Xu, J. Liang, J. Li, W. Yang, Tuning the Emission Properties of Ru(phen)32+ Doped Silica Nanoparticles by Changing the Addition Time of the Dye during the Stöber Process, Langmuir 26 (2010) 6657–6662, https://doi.org/10.1021/la903995r.
[55] S.V. Fedorenko, S.L. Grechkina, A.R. Mustafina, K.V. Kholin, A.S. Stepanov, I. R. Nizameev, I.E. Ismaev, M.K. Kadirov, R.R. Zairov, A.N. Fattakhova, R.R. Amirov, S.E. Soloveva, Tuning the non-covalent confinement of Gd(III) complexes in silica nanoparticles for high T1-weighted MR imaging capability, Colloid. Surf. B: Biointerfaces 149 (2017) 243–249, https://doi.org/10.1016/j.colsurfb.2016.10.025.
[56] A.R. Mukhametshina, A.R. Mustafina, N.A. Davydov, S.V. Fedorenko, I. R. Nizameev, M.K. Kadirov, V.V. Gorbatchuk, A.I. Konovalov, Tb(III)-doped silica nanoparticles for sensing: Effect of interfacial interactions on substrate-induced luminescent response, Langmuir 31 (2015) 611–619, https://doi.org/10.1021/la503074p.
[57] D.A. Freedman, S. Kruger, C.h. Roosa, C.h. Wymer, Synthesis, characterization and reactivity of $[Ru(bpy)(CH_3CN)_3(NO_2)]PF_6$, a synthon for $[Ru(bpy)(L_3)NO_2]$ complexes, Inorg. Chem. 45 (2006) 9558–9568, https://doi.org/10.1021/ic061039t.
[58] N. Chanda, D. Paul, S. Kar, S.M. Mobin, A. Datta, V.G. Puranik, K.K. Rao, G. K. Lahiri, Effect of 2-(2-pyridyl)azole-based ancillary ligands (L^{1-4}) on the electrophilicity of the nitrosyl function in $[Ru^{II}(trpy)(^{L1-}4)(NO^{]}]3+$ [trpy = 2,2‘: 6‘,2‘ ‘-terpyridine]. Synthesis, structures and spectroscopic, electrochemical and

kinetic aspects, Inorg. Chem. 44 (2005) 3499–3511, https://doi.org/10.1021/ic048184w.

[59] Q. Xiao, M. Zoulikha, M. Qiu, C. Teng, C. Lin, X. Li, M.A. Sallam, Q. Xu, W. He, The effects of protein corona on in vivo fate of nanocarriers, Adv. Drug Deliv. Rev.. 186 (2022), 114356, https://doi.org/10.1016/j.addr.2022.114356.

[60] J.A. Jackson, C. Turro, M.D. Newsham, D.G. Nocera, Oxygen quenching of electronically excited hexanuclear molybdenum and tungsten halide clusters, J. Phys. Chem. 94 (1990) 4500–4507, https://doi.org/10.1021/j100374a029.

[61] J.G. Elistratova, M.A. Mikhaylov, T.S. Sukhikh, K.V. Kholin, I.R. Nizameev, A. R. Khazieva, A.T. Gubaidullin, A.D. Voloshina, G.V. Sibgatullina, D.V. Samigullin, K.A. Petrov, M.N. Sokolov, A.R. Mustafina, Anticancer potential of hexamolybdenum clusters $[\{Mo_6I_8\}(L)_6]^{2-}$ (L = CF_3COO- and C_6F_5COO-) incorporated into different nanoparticulate forms, J. Mol. Liq. 343 (2021), 117601, https://doi.org/10.1016/j.molliq.2021.117601.

[62] E.V. Svezhentseva, Y.A. Vorotnikov, A.O. Solovieva, T.N. Pozmogova, I.V. Eltsov, A.A. Ivanov, D.V. Evtushok, S.M. Miroshnichenko, V.V. Yanshole, C.J. Eling, A. M. Adawi, J.-S.-G. Bouillard, N.V. Kuratieva, M.S. Fufaeva, L.V. Shestopalova, Y. V. Mironov, O.A. Efremova, M.A. Shestopalov, From photoinduced to dark cytotoxicity through an octahedral cluster hydrolysis, Chem Eur J 24 (2018) 17915–17920, https://doi.org/10.1002/chem.201804663.

[63] K. Kirakci, V. Sícha, J. Holub, P. Kubát, K. Lang, Luminescent hydrogel particles prepared by self-assembly of β-cyclodextrin polymer and octahedral molybdenum cluster complexes, Inorg. Chem. 53 (2014) 13012–13018, https://doi.org/10.1021/ic502144z.